



# THE FLOW-INDUCED VIBRATION OF A FLEXIBLE STRIP HANGING VERTICALLY IN A PARALLEL FLOW PART 1: TEMPORAL AEROELASTIC INSTABILITY

Y. YADYKIN, V. TENETOV AND D. LEVIN

*Faculty of Aerospace Engineering, Israel Institute of Technology Haifa 32000, Israel*

(Received 14 February 2000, and in final form 19 January 2001)

The effect of several parameters in a fluid–strip system are studied for linear/nonlinear models in detail. Such parameters are: the number of modes in the Galerkin discretization, the length of the strip, and the flow velocity. The present simulation clearly shows that when nonlinear forces are considered the response approaches a flutter-type limit cycle at supercritical flow speeds. The Reynolds number at which the strip begins to oscillate is about  $10^4$ – $10^5$ . With a further increase of the flow velocity the strip oscillates regularly. At higher flow velocities the oscillation becomes violent and irregular. The amplitude, frequency and drag coefficient at the limit cycle are presented as functions of the flow velocity for a given strip. The numerical predictions are in qualitative agreement with previous experimental data. © 2001 Academic Press

## 1. INTRODUCTION

THIS WORK CONSIDERS NONLINEAR fluid–structure interaction of a finite, flexible strip immersed in an otherwise homogeneous two-dimensional flow, as shown in Figure 1. The strip is fixed at the leading edge, and free at the other edges. The strip is a very thin flexible surface with a low aspect ratio, which allows us to model it as a thin plate with a very small bending stiffness.

The problem of the dynamic stability of an isolated flexible surface submerged in a uniform stream is quite old, dating back to Lord Rayleigh (1879), who studied the flapping of flags. Rayleigh attempted to explain the phenomenon of flutter by treating the flag as a massless and tension-free plane surface separating two half-spaces of moving air. He concluded that the flag is always unstable.

Thoma (1939) was probably the first to revert to this problem, half a century later, pointing out that the mass of the flag plays an important role. He treated the flag as an infinite membrane stretched by uniform tension forces. Thoma proved by a numerical example that lateral motion is possible in the form of a pair of traveling waves which satisfy the equations of motion and the shape of which resembles that of the fluttering flag.

For the particular problem of the flutter of a low aspect ratio membrane, fixed at both ends and surrounded by a uniform flow, both experimental and theoretical results were presented by Stearman (1959). His theoretical results did not predict all the experimentally observed types of flutter. The experiments reported by Stearman confirmed, only qualitatively, the theoretical result, by determining a critical velocity of the flow, at which a low-frequency flutter was observed, in the form of small-amplitude waves traveling downstream. However, at slightly higher velocities, a violent traveling-wave flutter, of larger amplitude and frequency, was observed. This large-amplitude flutter was attributed by

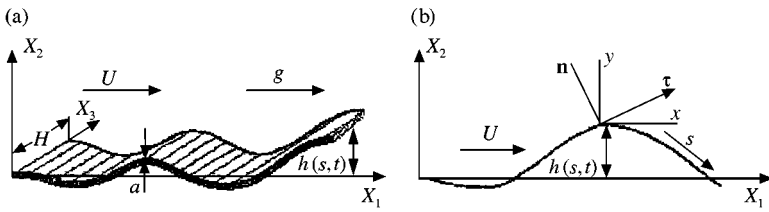


Figure 1. (a) Model of the system. (b) The coordinate systems.

other authors to the action of a three-dimensional flow (unaccounted for by the theory) which is especially significant in slender membranes (Kornecki 1978).

Systematic experiments with rectangular fabric strips suspended in a vertical air stream were reported by Taneda (1968), who found that when the strip does not flutter, the flow along the surface of the strip is laminar, and the wake of the strip forms a Karman vortex street. When the strip flutters, however, the flow separates from the surface, and is accompanied by a large-eddy wake and a consequent sharp rise in the amplitude and the drag force. The flow is very complicated at the trailing edge and the Kutta condition seems not to be satisfied. Taneda has shown that for very small flow speeds, the strip does not flutter at all. As the flow speed increases the trailing edge begins a flapping motion with small amplitude. The value of the critical Reynolds number at which the strip begins to oscillate is about  $10^4$ . This value seems to depend largely on the nature of the small initial disturbance, and to be nearly independent of the mass ratio and the Froude number. The strip flutters in various oscillation modes. With a further increase of the flow speed, the strip oscillates with regularity. At higher flow speeds the oscillation becomes violent and irregular. The regular periodic oscillation can be observed only at Reynolds numbers between  $10^4$  and  $10^5$  (Reynolds number is  $Ul/\nu$ , where  $U$  is the flow speed,  $l$  the length of strip and  $\nu$  the kinematic viscosity). The frequency of the strip motion increases with flow velocity. The smaller the strip length, the higher is the frequency, and the heavier the strip, the lower is the frequency. The amplitude and the drag increase abruptly at the critical Reynolds number.

The aeroelastic instability of a suspended slender plate clamped at its leading edge and stretched by the gravity forces and the aerodynamic friction drag (both vanishing at the free trailing edge) was investigated by Datta & Gottenberg (1975). The aerodynamic pressure perturbation was assumed according to the slender-body theory, and the problem was solved by a standard direct method using a modal series and Galerkin's technique. The derived governing equation of motion, with the aerodynamic forces being neglected, is similar to that of a suspended fluid-conveying pipe [e.g., Paidoussis & Issid (1974); Paidoussis (1998)]. Experiments, conducted on Mylar strips, showed a reasonable agreement with the theoretical results. In the limit of vanishing flexural rigidity of the plate, these results are valid for flags. Violent traveling-wave-type flutter was observed at certain critical flow velocities. However, in spite of available results, the flutter of flags is not yet fully understood (Kornecki 1978).

The first steps for investigating the nonlinear dynamics of a simply supported strip parallel to an ocean current were carried out by Triantafyllou (1983). The problem of the self-excited motions of such a strip was investigated analytically, using the aerodynamic theory of slender wings but without taking into account the bending stiffness of the strip. The stability boundaries of the strip were determined as a function of the external tension on it and the hydrodynamic parameters of the problem. Finally, the amplitude of the flutter motion was estimated by including the effect of the separation of the cross-flow.

More recently, Huang (1995) studied the flutter of cantilevered plates in an axial flow using a linear treatment suggested by Kornecki *et al.* (1976). The stability of the plate was investigated through an initial value problem. Theodorsen's classical solution was employed for the fluid loading. Viscosity was explicitly excluded, but its effect was embedded in the Kutta–Zhukovskii condition. The tension force on the plate was absent in this mathematical model. Huang adopted a linear analysis since he was interested mainly in the initial stage of the instability. A predictor–corrector numerical method was developed to simulate the transient process leading to the long-term periodic behavior. Wind tunnel experiments were carried out and were found to agree with the theory both qualitatively and quantitatively.

Thus, as indicated by Datta & Gottenberg (1975), the linear governing equation of motion of the suspended strip, with the aerodynamic forces being neglected, becomes similar to that of a cantilevered fluid-conveying pipe [e.g., Paidoussis & Issid (1974)]. This similarity remains valid also in the nonlinear case. In this latter case, the strip may be considered to be inextensible, and the nonlinearities are mainly geometrical, generated by the large curvature the strip assumes in the course of its arbitrary motions (Holmes 1977). The strip aerodynamic behavior is approximated by slender-body theory.

Most of the foregoing works have studied cantilever plates, or strips, with one fixed edge, disregarding the nonlinear effects of the fluid–structure interaction. The present paper attempts to take into account the influence of the nonlinear effects from both geometrical and aerodynamical sources on the strip dynamics.

## 2. DERIVATION OF THE EQUATION

The current derivation generalizes the planar linear equations of Datta & Gottenberg (1975) and the planar nonlinear equation of Lundgren *et al.* (1979) for a flexible strip hanging vertically in an axial flow (Figure 1).

The basic assumptions for the strip are as follows: (a) the strip has a uniform rectangular cross-section with length  $l$ , width  $H$ , constant mass per unit area  $m$ , and flexural rigidity  $D$ ; (b) the strip is long compared to its thickness  $a$  and its width  $H$ , and the effects of rotary inertia and shear deformation are ignored; (c) the center plane of the strip is inextensible; (d) the strip is elastic and initially straight; (e) a plane section before the deformation remains a plane during the deformation; (f) the effects of the internal dissipation of the strip material are neglected; (g) the motion is planar and the deflections of the strip  $h(s, t)$  are large, but the strains are small; (h) the strip is clamped at the upstream edge and is free at the downstream one.

The basic assumptions regarding the fluid flow are as follows: (a) the fluid is incompressible; (b) the incoming flow is uniform and of a constant velocity  $U$ .

In the undeformed state the strip extends along the  $X_1$ -axis of the Cartesian coordinate system  $(X_1 X_2 X_3)$  in the direction of gravity and oscillates in the  $(X_1 X_2)$  plane (Figure 1). Let  $(X_1, X_2, X_3)$  represent the position of a material point  $O$  in its original state, and  $(x, y, z)$  the position of the same material point in the deformed state. The displacement of that material point is defined as

$$v = x - X_1, \quad h = y - X_2, \quad w = z - X_3.$$

The strip, in its initially undeformed state lies along the  $X_1$ -axis, and when undergoing motions in the  $(X_1, X_2)$  plane, retains  $X_2 = 0$ , so that  $y$  is identical to the displacement  $h(s, t)$ , since the strip does not stretch. Thus, all the other physical quantities and the final governing equation can be expressed in terms of  $(s, t)$ . The strip plan-form is given by  $0 \leq s \leq l; 0 \leq z \leq H$ .

Let us introduce the orthogonal system of coordinates  $n, \tau$  connected to the strip (Figure 1). The  $n$  and  $\tau$  axes are normal and tangent to the center-plane of the strip, respectively.

The equations of motion in the  $v$ - and  $h$ -direction have been derived by Lundgren *et al.* (1979). When the aerodynamic drag force, as given by Hoerner (1975), is added, the equations of motion become

$$m \frac{\partial^2 v}{\partial t^2} + D \frac{\partial^4 v}{\partial s^4} - \frac{\partial}{\partial s} \left( (T - Dk^2) \frac{\partial v}{\partial s} \right) - m^* g - (\Delta p + F_n) \frac{\partial h}{\partial s} - F_\tau \frac{\partial v}{\partial s} = 0, \quad (1a)$$

$$m \frac{\partial^2 h}{\partial t^2} + D \frac{\partial^4 h}{\partial s^4} - \frac{\partial}{\partial s} \left( (T - Dk^2) \frac{\partial h}{\partial s} \right) + (\Delta p + F_n) \frac{\partial v}{\partial s} - F_\tau \frac{\partial h}{\partial s} = 0, \quad (1b)$$

where  $m = \rho_0 a$ ,  $m^* = (\rho_0 - \rho)a$ .

The pressure difference across the strip  $\Delta p$  was postulated in accordance with slender-wing theory (Katz & Plotkin 1991)

$$\Delta p = M \left( \frac{\partial}{\partial t} + U \frac{\partial}{\partial s} \right)^2 h(s, t) \quad (2)$$

and the curvature  $k$  is given by

$$k^2 = (\partial^2 v / \partial s^2)^2 + (\partial^2 h / \partial s^2)^2.$$

An additional equation is provided by the constraint on the length of the centerline,

$$(\partial v / \partial s)^2 + (\partial h / \partial s)^2 = 1. \quad (3)$$

The boundary conditions are

$$\begin{aligned} h = \partial h / \partial s = 0 & \quad \text{at } s = 0, \\ \partial^2 h / \partial s^2 = \partial^3 h / \partial s^3 = 0 & \quad \text{at } s = l. \end{aligned} \quad (4)$$

In equations (1)–(4),  $M = \rho \pi H / 4$  is the “added mass” of a cross-section of the strip per unit area (Datta & Gottenberg 1975). The values  $\rho_0, \rho$  are the densities of the strip material and the fluid, respectively,  $g$  is the acceleration due to gravity, and  $T$  is the tension force. The terms  $F_n, F_\tau$  are the normal and tangential aerodynamic forces acting on the strip by the flow. The normal aerodynamic force per unit area of the strip is defined, as proposed by Hoerner (1965, 1975) and Triantafyllou (1983), i.e.,

$$F_n = q(C_n U_R |U_R| + \frac{1}{2} \pi A U_R), \quad (5)$$

where  $q = \rho U^2 / 2$  is the dynamic pressure;  $A = H / l$  is the aspect ratio of the strip and  $U_R$  is the cross-flow component of the velocity. The notation  $U_R |U_R|$  was used in order to assure that the resulting force is in the direction of the cross-flow velocity (Triantafyllou 1983).

The nondimensional cross-flow component of the velocity is given by

$$U_R = \frac{(\partial h / \partial t + U \partial h / \partial s)}{U}. \quad (6)$$

The value of  $C_n$  in expression (5) is not known for the hydroelastic case. To a first—and rather crude—approximation,  $C_n$  can be considered equal to that of a rigid low aspect ratio wing inclined to the flow. In the case of rigid wings, the value of  $C_n$  is independent of the Reynolds number of the cross-flow, and depends only on the aspect ratio of the wing (Hoerner 1975). For the case of an infinitely long wing, i.e., zero aspect ratio,  $C_n$  is equal to

the drag coefficient of a flat plate, which is equal to two. The value of  $C_n$  decreases with increase in aspect ratio and approaches zero as the aspect ratio approaches infinity. Experimental values for  $C_n$  have been presented by Hoerner (1975), Triantafyllou (1983) and others for various aspect ratios. These values can be quantitatively estimated by the expression

$$C_n = C_0 e^{-A/2}, \tag{7}$$

where  $C_0 = 2, A < 1.0$ .

The tangential aerodynamic force per unit area of the strip is (Datta & Gottenberg 1975)

$$F_\tau = qC_\tau, \tag{8}$$

where the drag coefficient  $C_\tau$ , for a laminar flow, is given by Blasius (White 1991) as

$$C_\tau = 1.328\text{Re}_s^{-1/2} \tag{9}$$

and for a turbulent flow by White (1991) as

$$C_\tau = 0.054\text{Re}_s^{-1/7}. \tag{10}$$

Here  $\text{Re}_s = Us/\nu$  is the Reynolds number,  $s$  is a curvilinear coordinate along the strip,  $\nu$  is the kinematic viscosity of the fluid.

Equations (1) are coupled through the curvature  $k$ , axial force  $T$  and the aerodynamic forces  $F_n$  and  $F_\tau$ . In order to derive a single equation of motion in terms of  $h(s, t)$ , the first equation is integrated from  $s$  to  $l$ , divided by  $\partial v/\partial s$  to yield

$$T - Dk^2 = -\frac{1}{\sqrt{1-B}} \int_s^l (m\ddot{v} + Dv'''' - F_\tau v' - (\Delta p + F_n)h' - m^*g) ds, \tag{11}$$

where  $B = (h')^2$ . The dot and the prime denote the derivatives with respect to time  $t$  and to the curvilinear coordinate  $s$ , respectively.

By using condition (3) we can eliminate  $v$  and its derivatives via

$$v = \int_0^s \sqrt{1-B} ds, \quad \dot{v} = -\frac{1}{2} \int_0^s \frac{\dot{B}}{\sqrt{1-B}} ds, \quad \ddot{v} = -\frac{1}{2} \int_0^s \left( \frac{\ddot{B}}{\sqrt{1-B}} + \frac{\dot{B}^2}{(1-B)^{3/2}} \right) ds,$$

$$v' = \sqrt{1-B}, \quad v'' = -\frac{1}{2} \frac{B'}{\sqrt{1-B}}, \quad \left( \frac{h'}{\sqrt{1-B}} v'''' \right)' = -\left( \frac{h'}{\sqrt{1-B}} \left( \frac{B'}{2\sqrt{1-B}} \right)' \right)'. \tag{12}$$

Substituting equations (11) and (12) into (1b) a single equation describing the dynamics of the strip is obtained:

$$m\dot{h} + (\Delta p + F_n)\sqrt{1-B} + D \left[ h'''' + \frac{h'}{\sqrt{1-B}} \left( \frac{B'}{2\sqrt{1-B}} \right)' \right] - F_\tau h' + \left\{ \frac{h'}{\sqrt{1-B}} \int_l^s \left[ (\Delta p + F_n)h' + m^*g + F_\tau \sqrt{1-B} + \frac{m}{2} \int_0^s \left( \frac{\ddot{B}}{\sqrt{1-B}} + \frac{\dot{B}^2}{(1-B)^{3/2}} \right) dr \right] ds \right\}' = 0. \tag{13}$$

Equation (13) describes the flow-induced transverse vibration of a flexible strip hanging vertically in a parallel flow.

Removing the expression braces, in equation (13) may be rewritten as

$$\begin{aligned}
 m\dot{h} + \frac{(\Delta p + F_n + m^*gh')}{\sqrt{1-B}} + D \left( h''' + \frac{h'}{\sqrt{1-B}} \left( \frac{B'}{2\sqrt{1-B}} \right)' \right) \\
 + \frac{mh'}{2\sqrt{1-B}} \int_0^s \left( \frac{\dot{B}}{\sqrt{1-B}} + \frac{\dot{B}^2}{(1-B)^{3/2}} \right) ds - T(s, t)h'' = 0, \\
 T(s, t) = \frac{1}{(1-B)^{3/2}} \int_s^l ((\Delta p + F_n)h' + m^*g + F_\tau\sqrt{1-B}) ds \\
 + \frac{m}{2(1-B)^{3/2}} \int_s^l \int_0^s \left( \frac{\dot{B}}{\sqrt{1-B}} + \frac{\dot{B}^2}{(1-B)^{3/2}} \right) dr ds. \tag{14}
 \end{aligned}$$

For planar motions the transverse displacement is assumed to be “small” relative to the length of the strip, i.e.,  $h \approx O(\varepsilon)$ , where  $\varepsilon \ll 1$ . Small but finite strip rotations imply that  $B = (h')^2$  cannot be neglected compared to unity, whereas  $(h')^4$  and higher-order terms can. In this way, the general nonlinear equation of the strip motion (14) becomes

$$\begin{aligned}
 m\dot{h} + (\Delta p + F_n + m^*gh') \left( 1 + \frac{1}{2}h'^2 \right) + D[h''''(1 + h'^2) + 4h'h''h''' + h''^3] \\
 + mh' \int_0^s (\dot{h}'^2 + h'h'') ds - T(s, t)h'' + O(\varepsilon^5) = 0, \tag{15}
 \end{aligned}$$

where

$$\begin{aligned}
 T(s, t) = \left( 1 + \frac{3}{2}h'^2 \right) \int_s^l (m^*g + F_\tau) ds + \int_s^l (\Delta p + F_n)h' ds + m \int_s^l \int_0^s (\dot{h}'^2 + h'h'') dr ds + O(\varepsilon^4), \\
 \Delta p = \frac{\rho\pi H}{4} \left( \frac{\partial}{\partial t} + U \frac{\partial}{\partial s} \right)^2 h(s, t), \quad F_\tau = \frac{\rho U^2}{2} C_\tau, \\
 F_n = \frac{\rho}{2} C_n (\dot{h} + Uh') |\dot{h} + Uh'| + \frac{\rho U C_c}{2} (\dot{h} + Uh'), \quad C_c = \frac{\pi A}{2}.
 \end{aligned}$$

Equation (15) is similar to the equations of motion of pipes conveying fluid previously obtained [e.g., Semler & Paidoussis (1994)], except for the drag terms that exist in this equation, the external flow has a constant flow velocity, and the effect of the internal fluid mass is absent.

Equations (13–15) involve aerodynamic, elastic and inertial nonlinearities; see, e.g., Jensen (1997). A study of the separate influence of different nonlinearities on flexible strip motion is not examined in the framework of the present paper. In this regard, we must note that, strictly speaking, almost all nonlinearities in equations (13–15) are of geometrical nature (Kovacs & Ibrahim 1993) due to large deflections of the strip. The described classification of nonlinearities is conditional but it is often used (Grespo da Silva & Zaretsky 1990; Pai & Nayfeh 1990).

In equations (13–15), the aerodynamic nonlinearities  $m$  term  $F_n$  are of second order of magnitude, while all other terms are of higher order. If equations (15) are restricted to second order, we get the equation with one nonlinear term,  $F_n$  only. Numerical study shows that the aforesaid term  $F_n$  ensures the existence of flutter limit-cycle oscillation, cf. Triantafyllou (1983).

Estimations of the influence of the elastic and inertial nonlinearities are given in Grespo da Silva & Zaretzky (1990), Pai & Nayfeh (1990), Shyu *et al.* (1993), where the nonlinear characteristics of a cantilever beam change from “hard” to “soft” in the second mode. This is caused by the interaction between inertial and elastic nonlinearities. For the first mode the elastic nonlinearity dominates and yields a “hard” cubic nonlinearity. For the higher modes the inertial nonlinearity dominates and gives a “soft” cubic nonlinearity. Note that these results were obtained in the absence both of aerodynamic forces and gravity.

In our opinion the question of the combined influence of all three nonlinearities on strip motion is very delicate and difficult, and demands considerable research effort. We hope to devote additional attention to this question in the future.

Introducing next the nondimensional quantities:

$$\begin{aligned} \xi &= \frac{s}{l}, \quad \eta = \frac{h}{l}, \quad \tilde{\tau} = \left(\frac{D}{ml^4}\right)^{1/2} t, \quad V = \left(\frac{ml^2}{D}\right)^{1/2} U, \\ C_D(\xi) &= \frac{T(s, t)}{\rho U^2 l} - \left(1 + \frac{3(\eta')^2}{2}\right) \frac{m^* g}{\rho U^2} (1 - \xi), \\ \sigma &= \frac{\rho l}{2m}, \quad \gamma = \frac{m^* g l^3}{D}, \quad \delta = \frac{M}{m} \equiv \sigma C_c, \end{aligned}$$

the equation of motion (15) may be written in a nondimensional form as follows:

$$\begin{aligned} \ddot{\eta} + \eta'''' + [\eta'(\eta'\eta'')] + (\delta(\ddot{\eta} + 2V\dot{\eta}' + V^2\eta'') + \gamma\eta') \left(1 + \frac{\eta'^2}{2}\right) + \eta' \int_0^\xi (\dot{\eta}'^2 + \eta'\ddot{\eta}') d\xi \\ + \sigma [VC_c(\dot{\eta} + V\eta') + C_n(\dot{\eta} + V\eta')|\dot{\eta} + V\eta'|] \left(1 + \frac{\eta'^2}{2}\right) - T\eta'' + O(\varepsilon^5) = 0, \end{aligned} \tag{16}$$

where

$$\begin{aligned} T &= \sigma \left(1 + \frac{3}{2}\eta'^2\right) \int_\xi^1 \left(\frac{\gamma}{\sigma} + V^2 C_\tau\right) d\xi + \int_\xi^1 \int_0^\xi (\dot{\eta}'^2 + \eta'\ddot{\eta}') d\xi d\xi \\ &+ \sigma \int_\xi^1 \{VC_c(\dot{\eta} + V\eta') + C_n(\dot{\eta} + V\eta')|\dot{\eta} + V\eta'|\} \eta' d\xi \\ &+ \delta \int_\xi^1 (\ddot{\eta} + 2V\dot{\eta}' + V^2\eta'') \eta' d\xi + O(\varepsilon^4). \end{aligned} \tag{17}$$

In addition to the strip amplitude and the frequency of the limit cycle, there is also interest in the aerodynamic drag force (Taneda 1968). The aerodynamic drag force coefficient, per unit area of the wetted surface, may be written as follows:

$$\begin{aligned} 2C_D(\xi) &= \left(1 + \frac{3}{2}\eta'^2\right) \int_\xi^1 C_\tau d\xi + \frac{C_c}{V^2} \int_\xi^1 (\ddot{\eta} + 2V\dot{\eta}' + V^2\eta'') \eta' d\xi \\ &+ \frac{1}{V^2} \int_\xi^1 [VC_c(\dot{\eta} + V\eta') + C_n(\dot{\eta} + V\eta')|\dot{\eta} + V\eta'|] \eta' d\xi \\ &+ \frac{1}{\sigma V^2} \int_\xi^1 \int_0^\xi (\dot{\eta}'^2 + \eta'\ddot{\eta}') d\xi d\xi + O(\varepsilon^4). \end{aligned} \tag{18}$$

The total aerodynamic drag force coefficient per unit area of the wetted surface,  $C_D$ , may be obtained from equation (18) for  $\xi = 0$ :

$$2C_D(0) = \left(1 + \frac{3}{2}\eta'^2\right) \int_0^1 C_\tau d\xi + \frac{C_c}{V^2} \int_0^1 (\ddot{\eta} + 2V\dot{\eta}' + V^2\eta'')\eta' d\xi + \frac{1}{V^2} \int_0^1 [VC_c(\dot{\eta} + V\eta') + C_n(\dot{\eta} + V\eta')|\dot{\eta} + V\eta'|]\eta' d\xi + \mathcal{O}(\varepsilon^4). \tag{19}$$

Now equation (16) is to be solved, subject to the following boundary conditions:

$$\eta = \eta' = 0 \quad \text{at } \xi = 0, \quad \eta'' = \eta''' = 0 \quad \text{at } \xi = 1. \tag{20}$$

### 3. METHOD OF SOLUTION

We have applied a standard method, based on Galerkin’s technique, for the numerical solution of equation (16); see, for example, Datta & Gottenberg (1975). The solution is represented by the series

$$\eta(\tilde{\tau}, \xi) = \sum_{j=1}^{\infty} Q_j(\tilde{\tau}) \Phi_j(\xi), \tag{21}$$

where  $\eta$  is expanded in terms of the eigenfunctions of the equation

$$\Phi^{iv} - \lambda^4\Phi = 0, \tag{22}$$

satisfying boundary conditions (20). The eigenvalues  $\lambda_j$  are given by  $\lambda_j = 1.8751, 4.69409, 7.85476$ , etc., and the corresponding normalized eigenfunctions are

$$\Phi_j = \cosh \lambda_j \xi - \cos \lambda_j \xi - \alpha_j(\sinh \lambda_j \xi - \sin \lambda_j \xi)$$

with  $\alpha_j = (\cosh \lambda_j + \cos \lambda_j)/(\sinh \lambda_j + \sin \lambda_j)$ . These functions obey the orthonormality relations

$$\int_0^1 \Phi_i \Phi_j d\xi = 0, \quad i \neq j, \quad \int_0^1 \Phi_i \Phi_j d\xi = 1, \quad i = j.$$

As shown previously [e.g. Semler & Paidoussis (1996)], equation (16) is reduced to a set of second-order nonlinear differential equations of the type

$$M_n \ddot{Q} + B_n \dot{Q} + K_n Q = F(\ddot{Q}, \dot{Q}, Q, \tilde{\tau}), \tag{23}$$

where  $Q$ ,  $M_n$ ,  $B_n$ ,  $K_n$  are the generalized displacement, mass, damping and stiffness, respectively;  $F$  is the nonlinear function of the elastic, dissipative and inertia forces.

In order to use the numerical procedure of solution for the system, it is necessary to express (23) in a normal form  $\dot{y} = \tilde{F}(y, t)$ ,  $y(0) = y_0$ .

This problem is solved in two steps: reduction of the system order by a standard replacement of variables, and a numerical determination of  $\ddot{Q}$  where necessary, in the process of the numerical integration to obtain the normal form. We used the Gear method (Gear & Petzold 1984) for the numerical integration and the modified Powell method (More *et al.* 1980) for determining  $\ddot{Q}$  in the procedure of calculation, for the derived right part of the normal form. The solution, equation (21), is used in the form

$$\eta(\tilde{\tau}, \xi) = \sum_{j=1}^N Q_j(\tilde{\tau}) \Phi_j(\xi), \quad \text{where } N \geq 2. \tag{24}$$

The selection of the required value for  $N$ , is a subtle question, as shown in the following, and is a topic for discussion. A numerical study has indicated that a physical time of 12 s was sufficient for the development of the oscillation process. The results shown below are obtained during 1 s of oscillations, usually between the 11th and 12th seconds. There exist enough data about the process within 1 s to acquire confidence in the nature of the solution.

## 4. NUMERICAL RESULTS AND DISCUSSION

### 4.1. GENERAL NATURE OF RESULTS

In order to establish confidence in the present mathematical model for strip motion, equation (16), a numerical study was conducted. The principal difficulty is that the number of modes required for a given desired accuracy increases (and consequently also the computation time) as the aspect ratio decreases. The convergence problem is further discussed in the next section.

A typical flutter computation time is of the order of 10 min for eight modes on the PC Pentium II (Intel 200 MHz, 64 MB RAM).

In general, the behavior of the strip response can be described as follows. For velocities lower than the critical speed, the strip oscillations display spatiotemporal decay. At speeds higher than the critical one, the oscillations display flutter with temporal amplification of the amplitude until a limit cycle is obtained.

All results have been obtained for the following initial conditions:

$$h_1(0) = a, \quad h_j(0) = 0, \quad \dot{h}_j(0) = 0, \quad j = 2, 3, \dots, N, \quad (25)$$

where  $N$  is the number of eigenmodes in expansion (24).

### 4.2. THE HOPF BIFURCATION

The system parameters for the strip are chosen as follows: the density of air  $\rho = 1.07 \text{ kg/m}^3$ ; the density of strip  $\rho_0 = 3900 \text{ kg/m}^3$ ; the flexural rigidity of the strip  $D = 323a^3 \text{ MN/m}^2$ ; the kinematic viscosity of the air  $\nu = 0.15 \text{ cm}^2/\text{s}$ ; the thickness of the strip  $a = 0.05 \text{ mm}$ ; the length  $l$  of the strip is varied between 0.1 and 1.0 m; the width  $H = 0.025 \text{ m}$ ; and the flow velocity  $U$  is gradually increased.

For high enough  $U$  the hitherto stable static equilibrium is lost, giving birth (if nonlinearities are taken into account) to a stable limit cycle. This defines a Hopf bifurcation (Holmes 1977), or flutter in aerolastic terminology. The critical value  $U$  for the Hopf bifurcation may be found by solving the eigenvalue problem of the linearized system (Datta & Gottenberg 1975). However, the nonlinear treatment is of interest in two respects. In the first place, it enables us to evaluate the amplitudes of the deflections and the total drag force when the critical flutter velocity is exceeded. Secondly, it is to be expected that the nonlinearity of the aerodynamic forces can introduce new aerolastic effects not observed at moderate velocities. These aspects of the problem have been considered by Bolotin (1963); that work deals in particular with examples of problems in which the aerodynamic forces are able to maintain undamped motion at velocities less than the critical velocities determined by the linear theory, when a large enough disturbance acts on the system. In such cases the critical velocity determined by the methods of the linear theory of aeroelasticity is only the upper limit of the critical velocities for actual structures.

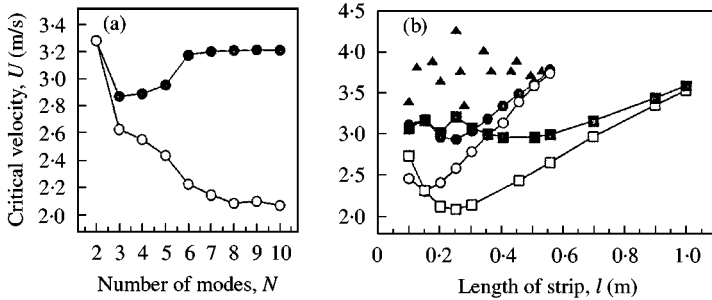


Figure 2. The calculated critical flow velocity for the Hopf bifurcation as a function of: (a) the number of modes,  $N$ , in the Galerkin discretization for linear (—●—) and nonlinear (—○—) models; (b) the length of the strip,  $l$ , for linear (—●—,  $N = 4$ ; —■—,  $N = 8$ ) and nonlinear (—○—,  $N = 4$ ; —□—,  $N = 8$ ) models; ▲, the experimental results by Datta & Gottenberg (1975).

#### 4.3. RESULTS AND DISCUSSION

In the numerical results presented in Figure 2(a) the number of terms in expansion (24) were varied from  $N = 2$  to 10. The length of the strip was  $l = 0.25$  m. The values of the critical velocity computed by the nonlinear equation became appreciably less than those of the linear equation. Note that starting with a certain number of modes in expansion (24) the variation of the computed critical velocity is small. This number of modes is six for the linear case and eight for the nonlinear case.

Figure 2(b) presents the results of the numerical solutions of the linear and nonlinear equations for  $N = 4$  and 8 in expansion (24). Presented here are the values of the critical velocity versus the strip length. The experimental results of Datta & Gottenberg (1975) are also presented.

It ought to be mentioned that the critical air velocities were determined by Datta & Gottenberg (1975) in two ways: “first, visual observation of the test strip revealed virtually no motion well below the critical speed, some tendency at times to oscillate with increasing amplitude as air speed increased, and finally a violent oscillation with the free end of the strip reaching the tunnel walls just as the critical speed was attained; second all these disturbances were sensed by a force transducer with a recorder pen being suddenly driven off scale in the y-axis direction at the critical speed”. Evidently, the critical velocity was fixed by Datta & Gottenberg in two ways for violent oscillations with the free end of the strip reaching the tunnel walls. These oscillations arose at a flow velocity higher than the critical one. The computations for  $N = 8$  (see below) show that the flow velocity of violent oscillations lies beyond the critical velocity and is larger than 3.08 m/s.

The numerical results show that there are distinctions in the level of the solution: the stability boundary of the nonlinear system lies below the stability boundary of the linear system. The difference in the values of the critical velocity for a given length of the strip, as determined by linear and nonlinear theory, is attributable to the effect of the initial condition (Reynolds & Dowell 1993). This difference in the critical velocities decreases when increasing the length of the strip.

Figure 3 shows the sensitivity to initial conditions for the strip motion. The results are presented for the flow velocity  $U = 2.125$  m/s, strip length  $l = 0.25$  m and the following initial conditions:

$$\begin{aligned} & \text{(a) } h_1(0) = 100a, \quad \text{(b) } h_1(0) = a, \quad \text{(c) } h_1(0) = 0.01a; \text{ and} \\ & h_j(0) = 0, \quad j = 2, 3, \dots, N, \quad \dot{h}_j(0) = 0, \quad j = 1, 2, \dots, N, \text{ in all cases,} \end{aligned} \quad (26)$$

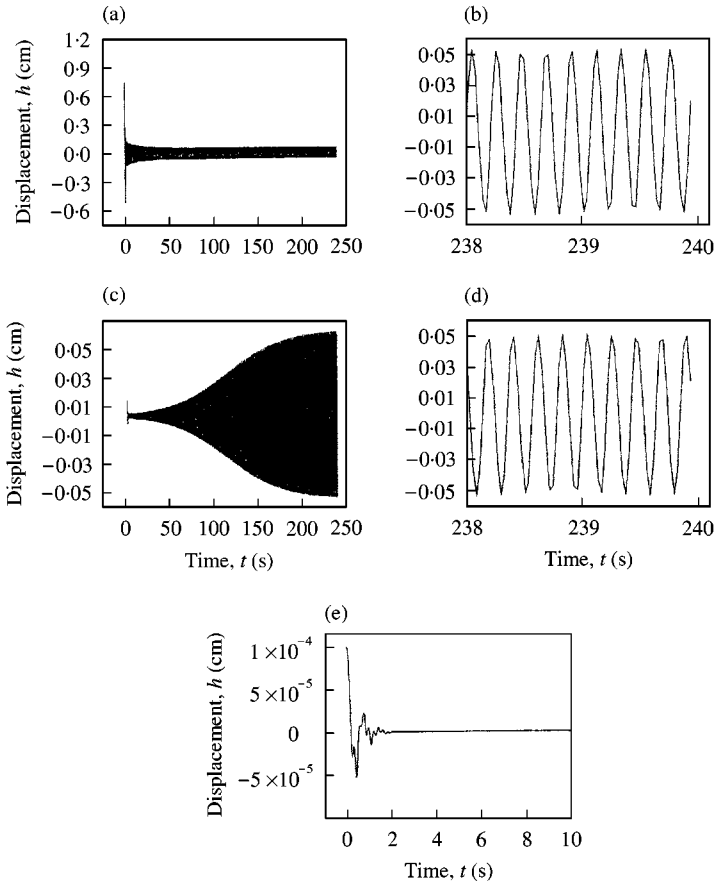


Figure 3. The free-end behavior of the strip for three variants of initial conditions: (a, b)  $h_1 = 100a$ ; (c, d)  $h_1 = a$ ; (e)  $h_1 = 0.01a$ ; (a, c, e) give the full time history; (b, d) show the last 2 s.

where  $a$  is the strip thickness. An analogous type of set of initial conditions is generally accepted (Bolotin 1963; Ventres & Dowell 1970; Paidoussis *et al.* 1991).

An initial deflection of the order of the strip thickness or more is physically equivalent to a large disturbance of a strip [Figure 3(a–d)]. This “large disturbance” allows us to find from equation (15) the boundary of flutter-like oscillations below the linear flutter boundary (Figure 2). All the calculations for the so-called “large disturbance” indicate that the limit-cycle characteristics (amplitude, frequency) generally do not depend on the initial conditions (Ventres & Dowell 1970; Paidoussis *et al.* 1991; Paidoussis 1998).

A deflection of the order of  $0.01a$  or less is physically equivalent to a small disturbance [Figure 3(e)] and allows us to find the flutter boundary close to the linear flutter boundary. Figure 3 shows an increase of critical velocity in the direction of the boundary of the linear stability as the initial strip deflection decreases.

Unfortunately, we did not find from equation (15) the exact threshold of the initial condition, below which the system is stable until the linear flutter velocity is reached, and above which the system goes to a limit-cycle oscillation.

The decrease of the above-mentioned difference in the critical velocities when increasing the strip length, as shown in Figure 2(b), may be attributed to the following. The normal aerodynamic force  $F_n$  has a “hard” nonlinearity (Bolotin 1963), in the sense that the sign of

the nonlinear contribution coincides with the sign of the cross-flow component of the velocity  $U_R$  [equation (5)]. Bolotin (1963) showed that whenever the aerodynamic forces have a “hard” nonlinearity, their effect on the behavior of an elastic system will be essentially opposite to the effect of an elastic nonlinearity. An increase in the elastic nonlinearity causes a reduction in amplitude in the case of a steady flutter. Whenever there is a considerable elastic nonlinearity, the excitation of a flutter on the boundary of the instability region will be “soft”, in the sense that if the critical velocity is slightly exceeded, the amplitudes of steady flutter will be small. In other words, the stability boundary will be “safe”. Conversely, when the aerodynamic nonlinearity predominates, the excitation of oscillations on the boundary of the instability region can be “hard”, and the boundary of the stability region becomes “unsafe”. In this case, the aerodynamic forces can maintain states of motion other than the undisturbed state, even when the undisturbed motion is stable with respect to small disturbances. Hence, the critical velocities determined from the linearized equations are the upper critical velocities (Figure 2). The lower critical velocities we can define as velocities at which the excitation of a steady flutter motion becomes possible. Thus, the elastic nonlinearity in the relationship between the longitudinal strain and the transverse displacement of the flexible strip causes a reduction in flutter amplitude and belongs to the “hard” type; however, the effect of inertia and aerodynamic nonlinearities on the behavior of the strip will be essentially the opposite.

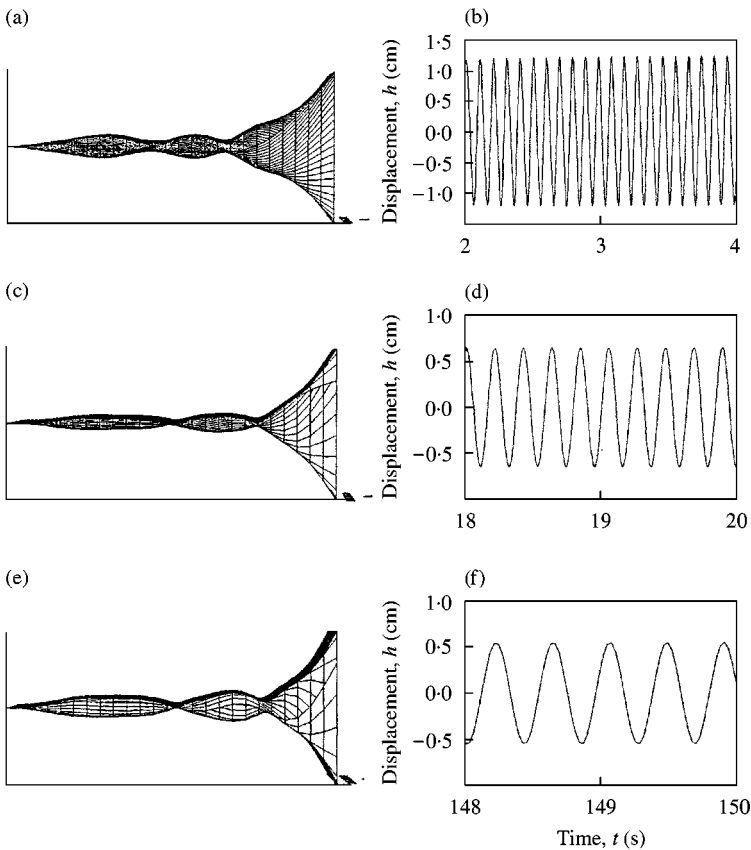


Figure 4. (a, c, e) The streamwise envelope of the fluttering strip and (b, d, f) corresponding limit-cycle oscillation parameters (displacement and frequency) of the free strip edge for different values of strip length  $l$  and flow velocity  $U$ ; (a, b)  $l = 0.1$  m,  $U = 2.75$  m/s; (c, d)  $l = 0.25$  m,  $U = 2.2$  m/s; (e, f)  $l = 1.0$  m,  $U = 3.7$  m/s.

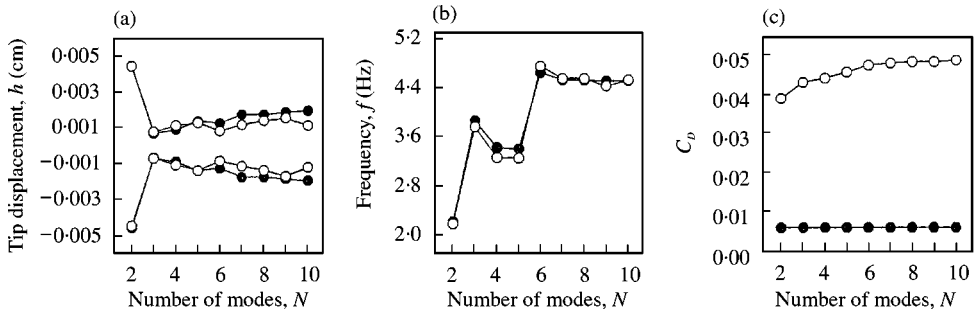


Figure 5. Variation of the oscillation parameters ( $h$ ,  $f$ , and  $C_D$ ) versus the number of modes,  $N$ , for the corresponding critical flow velocities: —●—, linear model; —○—, nonlinear model.

The gravity force  $m^*g$  and the tangential aerodynamic forces  $F_t$  increase the strip tension [equation (14)] and thereby cause a reduction in the flutter amplitude (Paidoussis 1970). This effect is opposite [equation (13)] to both inertial and aerodynamic nonlinearities and depends upon the strip length. The correlation of the foregoing forces changes the nonlinear characteristics of the strip from “soft” to “hard” type as the strip length is increased. Indeed, with increasing strip length, the sensitivity of the strip to flutter at the pre-critical velocities rapidly decreases. This leads to a decrease in the difference between the results (the stability boundary) by linear and nonlinear theories as the strip length increases (Figure 2). Note that “hard” excitation takes place for the strip with the nonlinear characteristics of the “soft” type and, on the other hand, “soft” excitation takes place for the strip with the nonlinear characteristics of the “hard” type (Bolotin 1963).

Figure 4(a, c, e) shows that an increase of the strip length from 0.1 to 1 m slightly changes the streamwise envelope of the fluttering strip immediately after the critical velocity is reached. At the same time, Figure 4(b, d, f) shows a decrease of the amplitude and frequency of the fluttering strip, each being a result of the decrease in the effects of both the inertial and the aerodynamic nonlinear forces, leading to a “soft” excitation of the flutter on the boundary stability. The nonlinear boundary of the stability comes closer to the linear one (Figure 2).

In Figure 5(a–c), three sets of curves are presented to show the dependence of the computed results on the number of modes in expansion (24) in the numerical solution of the linear and the nonlinear equation (16). The computed results of the tip displacement  $h$ , the frequency of oscillation  $f$ , and the coefficient  $C_D$  are shown, respectively, for the strip length  $l = 0.25$  m and at the critical air speeds, corresponding to the number of modes in expansion (24) [see Figure 2(a)]. The results show a large variance when the number of modes is smaller than seven. The nonlinear solutions for the tip displacement and the frequency are close to those of linear theory; however, not surprisingly, the computed  $C_D$  is much higher in the nonlinear solution.

The tip displacement, frequency and drag coefficient of the fluttering strip computed by equation (16) at air speed  $U = 3.75$  m/s, which well exceeds the critical velocity, are presented in Figure 6 for a varying number of modes. Figure 6 shows that for number of modes larger than five the calculated characteristics of the oscillations are irregular. The oscillations may be considered chaotic in this case.

The results for the strip ( $l = 0.25$  m,  $H = 0.025$  m) with an initial disturbance  $h = a$  are represented in Figure 7. The calculations were for  $N = 8$  in expansion (24). The columns (a, b, c) correspond to subcritical ( $U = 2.0$  m/s), critical ( $U = 2.1$  m/s) and supercritical ( $U = 2.2$  m/s) air velocities, respectively. The upper plots show the horizontal displacement

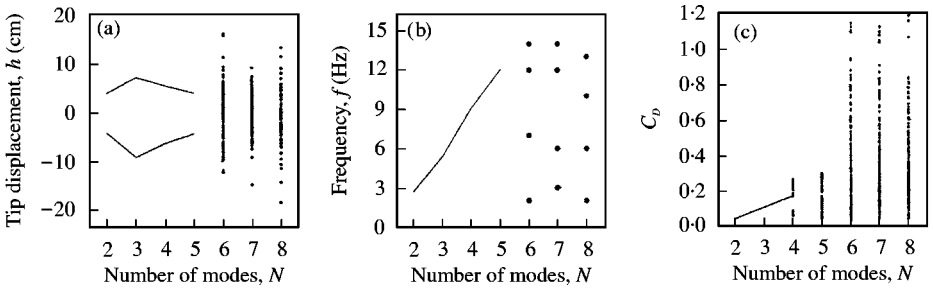


Figure 6. Variation of the oscillation parameters ( $h$ ,  $f$ , and  $C_D$ ) for a supercritical flow velocity,  $U = 3.75$  m/s, with increasing number of modes,  $N$ , for the nonlinear model of the fluttering strip.

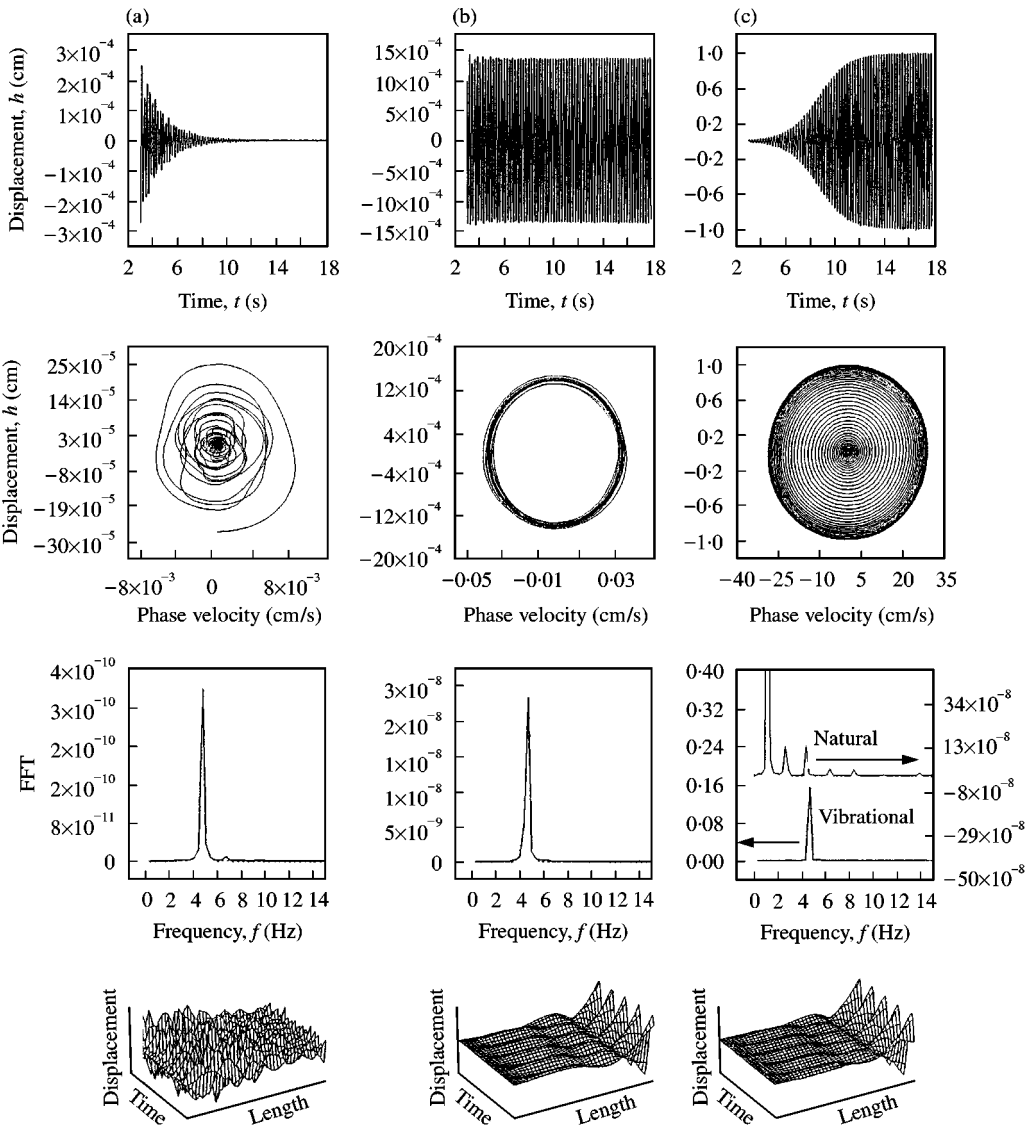


Figure 7. Three simulations: (a) subcritical,  $U = 2.0$  m/s, (b) critical,  $U = 2.1$  m/s, (c) supercritical,  $U = 2.2$  m/s, and the natural frequencies (at  $U = 0.1$  m/s), for a strip with  $l = 0.25$  m,  $H = 0.025$  m.

as a function of time. Note the difference in scales. The corresponding projections of the phase space are shown in the second row. In the third row the results of the Fourier analysis of the strip oscillations are represented. The lowermost row contains 3-D plots to illustrate the wave structure of the strip behavior.

Column (a) shows that the motion is clearly decaying and the fast Fourier transform (FFT) clearly indicates the presence of two frequencies. The projection of the phase space clearly resembles a stable focus (Andronov *et al.* 1966). There is no damping in the structural model (16); therefore, if there were no aerodynamic damping, the simulated motion would persist forever. However, the aerodynamic model provides damping through radiation of energy to infinity along the wake behind the strip, although viscosity does not appear explicitly in the aerodynamic damping forces. In column (b) of Figure 7 the response to an initial disturbance very close to the critical air velocity is shown. It seems that a limit cycle has developed instead of a stable focus, and the two distinct frequencies, shown in column (a), have now merged. The merged frequency lies between the two previous frequencies from column (a), thus indicating a coalescence in natural frequencies, typical of coupled-mode flutter. However, the amplitude of the apparent limit cycle and frequency depend on the initial condition. Most likely, therefore, the response is not truly a limit cycle, but either a very slightly stable or very slightly unstable focus (Preidikman & Mook 1997).

The response to an initial disturbance at a supercritical air speed is shown in column (c). Again there is only one frequency as in column (b), but now a stable limit cycle appears in the phase plane instead of an unstable one. The frequency is near the natural frequency of the third mode [Figure 7(c)]. The process of transition to a stable limit cycle of oscillations is relatively slow and takes about 12 s approximately.

In simulations such as the current one, the flow serves as either an infinite source of energy or an infinite sink. At subcritical velocities the airstream absorbs energy from the strip and damps its motion; at supercritical velocities it excites the strip and the amplitude of the motion grows and approaches the amplitude of a stable limit cycle. Here the response of the strip is a true limit cycle as shown in Figure 7(c).

In the bottom row the space-time illustration of the wave structure for the strip behavior is presented. In the subcritical range we can see that the wave motion is clearly decaying along the strip towards the free edge [Figure 7(a)]. The process is a multiwave one. Contrary to the subcritical case, in the critical and the supercritical cases the wave structure is that of a standing wave [Figure 7(b, c)]. The amplitude of the wave increases towards the free edge. Taneda (1968) observed similar results for vertically hanging flags.

Three sets of the calculated parameters in a wide range of post-critical velocity domain are shown in Figure 8(a-c). The upper plots show the tip displacement  $h$ , the frequency  $f$  of the oscillation of the free edge and the total drag coefficient  $C_D$ , respectively, versus the flow velocity. The lower row shows the dependence of the three aforementioned parameters on the flow velocity in the vicinity of an air speed of  $U = 2.38$  m/s. The calculations were carried out for the previously noted example and for  $N = 8$  in expansion (24). The flutter computation time, of one variant, is in the order of 10 min for  $N = 8$ . The calculations are computed for 12 s of the simulated motion.

The results in Figures 7 and 8 show that four distinct types of solution may occur, as follows.

(i) Solutions converging to a stable equilibrium for subcritical air velocities ( $U < 2.1$  m/s), [Figure 8(a)]. The wave motion is decaying along the strip towards the free edge [Figure 7(a)].

(ii) Periodic solutions, corresponding to regular oscillations, whose above-mentioned parameters slowly increase on increasing the air velocity from 2.1 to 2.38 m/s [Figure 8(a)].

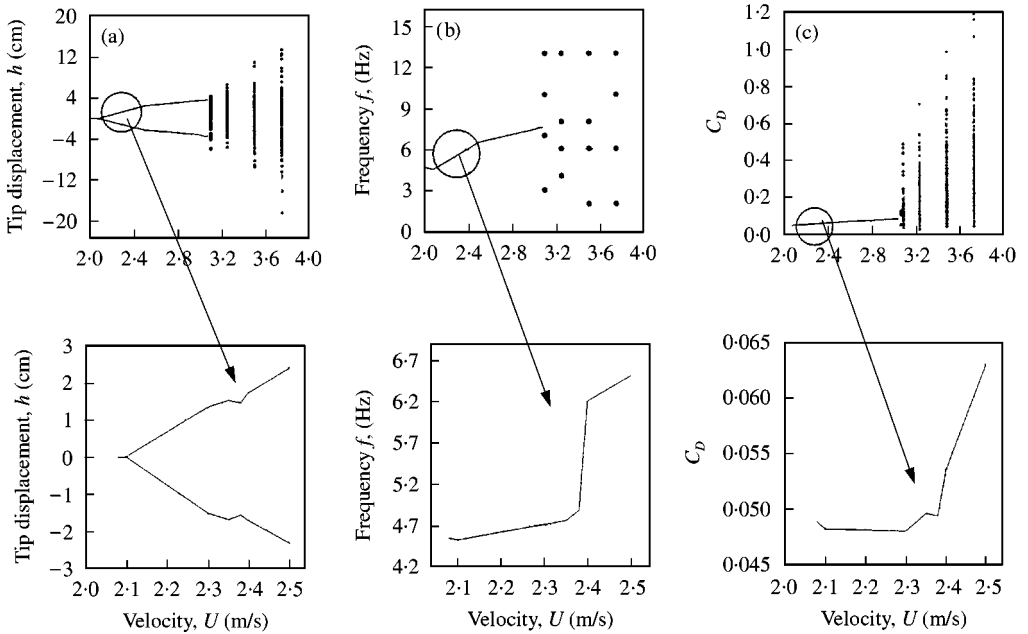


Figure 8. Dependence for the calculated parameters of the fluttering strip, showing (a)  $h$ , (b)  $f$ , (c)  $C_D$  as a function of  $U$ , for  $N = 8$ ; lower row shows an enlargement of the circled areas in the upper figures.

The envelope of the amplitudes of the strip motion along the strip has a shape which is close to that of a standing wave [Figure 7(b, c)]. A jump in the response ( $h$ ,  $f$ ,  $C_D$ ) occurs at  $U = 2.38$  m/s.

(iii) Periodic solutions corresponding to regular oscillations take place for a further increase of the flow velocity until  $U = 3.08$  m/s. The envelope of the amplitudes of the strip motion also has a shape which is close to that of a standing wave. The jump-like transition from regular oscillations to irregular motions takes place at  $U = 3.08$  m/s.

(iv) Irregular oscillations for air velocities higher than  $U = 3.08$  m/s. The solutions acquire the shape of traveling waves along the strip in the direction of the trailing edge. The steep change in the response of the calculated parameters is even steeper at  $U = 3.08$  m/s than the one observed at  $U = 2.38$  m/s.

Thus for small flow velocities,  $U < 2.1$  m/s, the strip does not flutter at all. As the flow velocity is increased and reaches the critical speed  $U \approx 2.1$  m/s, the trailing edge of the strip begins a flapping motion with small amplitude and constant frequency. Further increase of the flow velocity increases both the amplitude and the frequency of the regular oscillations. At higher flow velocity,  $U > 3.08$  m/s, the oscillations become violent and irregular. This is in agreement with the observations of Datta & Gottenberg (1975). The transition from regular to irregular oscillations occurs as a jump in the parameters of motion at  $U = 3.08$  m/s. The character of the regular oscillations is of a standing-wave type, while the irregular oscillations have a traveling-wave characteristic.

The present simulations predict the onset and the evolution of flutter of the strip in qualitative agreement with the experimental work (Taneda 1968; Datta & Gottenberg 1975), and is consistent with the assertion of Bolotin (1963) as to the effect of nonlinear terms in the simulation.

## 5. SUMMARY AND CONCLUSIONS

A nonlinear mathematical model has been developed in order to study the evolution of disturbances in a finite, flexible strip hanging vertically and subjected to a uniform parallel flow. A series of numerical experiments have been conducted for the linear/nonlinear model for various strip lengths. The study was focused on the range of flow velocities at which small initial disturbances begin to develop into an aeroelastic instability that leads to a limit-cycle oscillation. In the range of the fluid–structure parameters that were studied, eight modes should be employed to obtain quantitative accuracy.

The main conclusions obtained by the present study are as follows. For small flow velocities the strip does not flutter at all. As the flow velocity is increased, the trailing edge of strip begins a regular flapping motion with small amplitudes. The strip oscillates regularly with a standing-wave type of motion. A further increase of the flow velocity leads to a steep jump of the parameters of the flapping motion. However, the strip continues to flap regularly, in this range, with a standing-wave type of oscillation. At a higher flow velocity, a second jump in the parameters of the motion occurs. However, at this velocity the nature of the oscillation changes into a nonregular, traveling wave in the direction of the trailing edge. No further significant change in the strip response at higher flow velocities has been observed.

The present numerical study predicts the onset and the evolution of flutter of the strip. Although the present simulations provide mainly a solution in the time domain, the comprehensive model of the strip motion in the flow also allows one to study the wave structure.

## ACKNOWLEDGEMENT

The authors wish to acknowledge the financial support given to this work by: The Center for Absorption in Science, Ministry of Immigrant Absorption, State of Israel. The authors would also like to thank the reviewers for their useful comments.

## REFERENCES

- ANDRONOV, A. A., VITT, A. A. & KHAIKIN, S. E. 1966 *Theory of Oscillators*. New York: Pergamon Press.
- BOLOTIN, V. V. 1963 *Nonconservative Problems of the Theory of Elastic Stability*. New York: Pergamon Press.
- DATTA, S. K. & GOTTENBERG, W. G. 1975 Instability of an elastic strip hanging in an airstream. *Journal of Applied Mechanics* **42**, 195–198.
- GEAR, C. W. & PETZOLD, L. R. 1984 ODE methods for the solutions of differential/algebraic systems. *SIAM Journal Numerical Analysis* **21**, 716–728.
- GRESPO DA SILVA, M. R. M. & ZARETZKY, C. L. 1990 Non-linear modal coupling in planar and non-planar responses of inextensional beams. *International Journal of Non-Linear Mechanics* **25**, 227–239.
- HOERNER, S. F. 1965 *Fluid-Dynamic Drag. Practical Information on Aerodynamic Drag and Hydrodynamic Resistance*. Brick Town, NJ: published by the author.
- HOERNER, S. F. 1975 *Fluid-Dynamic Lift. Practical Information on Aerodynamic and Hydrodynamic Lift*. Brick Town, NJ: published by L.A. Hoerner.
- HOLMES, P. J. 1977 Bifurcations to divergence and flutter in flow-induced oscillations: a finite dimensional analysis. *Journal of Sound and Vibration* **53**, 471–503.
- HUANG, L. 1995 Flutter of cantilevered plates in axial flow. *Journal of Fluids and Structures* **9**, 127–147.
- JENSEN, J. S. 1997 Fluid transport due to nonlinear fluid–structure interaction. *Journal of Fluids and Structures* **11**, 327–344.
- JONES, R. T. 1946 Properties of low-aspect ratio pointed wings at speeds below and above the speed of sound. Technical Report 835, NASA.

- KATZ, J. & PLOTKIN, A. 1991 *Low-Speed Aerodynamics*. New York: McGraw-Hill.
- KORNECKI, A. 1978 Aeroelastic and hydroelastic instabilities of infinitely long plates 1. *Solid Mechanics Archives* **3**, 381–439.
- KORNECKI, A., DOWELL, E. H. & O'BRIEN, J. 1976 On the aeroelastic instability of two-dimensional panels in uniform incompressible flow. *Journal of Sound and Vibration* **47**, 163–178.
- KOVACS, A. P. & IBRAHIM, R. A. 1993 Relationship between multibody dynamics computation and nonlinear vibration theory. *Nonlinear Dynamics* **4**, 635–653.
- LUNDGREN, T. S., SETHNA, P. R. & BAJAJ, A. K. 1979 Stability boundaries for flow induced motions of tubes with an induced terminal nozzle. *Journal of Sound and Vibration* **64**, 553–571.
- MORE, J., GARBOW, B. & HILLSTROM, K. 1980 User guide for MINPACK-1, Argonne National Labs Report ANL-80-74, Argonne, IL, U.S.A.
- PAIDOUSSIS, M. P. 1970 Dynamics of tubular cantilevers conveying fluid. *IMechE Journal of Mechanical Engineering Science* **12**, 85–103.
- PAIDOUSSIS, M. P. 1998 *Fluid-Structure Interactions: Slender Structures and Axial Flow*, Vol. 1. London: Academic Press.
- PAIDOUSSIS, M. P. & ISSID, N. T. 1974 Dynamic stability of pipes conveying fluid. *Journal of Sound and Vibration* **33**, 267–294.
- PAIDOUSSIS, M. P., LI, G. X. & RAND, R. H. 1991 Chaotic motions of a constrained pipe conveying fluid: comparison between simulation, analysis and experiment. *Journal of Applied Mechanics* **58**, 559–565.
- PAI, P. F. & NAYFEH, A. H. 1990 Non-linear non-planar oscillations of a cantilever beam under lateral base excitations. *International Journal of Non-Linear Mechanics* **25**, 455–474.
- PREIDIKMAN, S. & MOOK, D. T. 1997 Numerical simulation of flutter of suspension bridges. *Applied Mechanics Reviews* **50** (Part 2), S174–S179.
- RAYLEIGH. 1879 On the instability of jets. *Proceedings of the London Mathematical Society* **10**, 4–12.
- REYNOLDS, R. R. & DOWELL, E. H. 1993 Nonlinear aeroelastic response of panels. AIAA-93-1599-CP, 2566–2576.
- SEMLER, C., LI, G. X. & PAIDOUSSIS, M. P. 1994 The non-linear equations of motion of pipes conveying fluid. *Journal of Sound and Vibration* **169**, 577–599.
- SEMLER, C. & PAIDOUSSIS, M. P. 1996 Nonlinear analysis of the parametric resonance of a planar fluid conveying cantilevered pipe. *Journal of Fluids and Structures* **10**, 787–825.
- SEMLER, C., GENTLEMAN, W. C. & PAIDOUSSIS, M. P. 1996 Numerical solutions of second order implicit non-linear ordinary differential equations. *Journal of Sound and Vibration* **195**, 553–574.
- SHYU, I.-M. K., PLAUT, R. H. & MOOK, D. T. 1993 Whirling of a forced cantilevered beam with static deflection. II: Superharmonic and subharmonic resonances. *Nonlinear Dynamics* **4**, 337–356.
- STEARMAN, R. 1959 Small aspect ratio panel flutter. California Institute of Technology, Report AFOSR-TR 1, 59–45.
- TANEDA, S. 1968 Waving motions of flag. *Journal of the Physical Society of Japan* **24**, 393–401.
- THOMA, S. 1939 Why does the flag flutter. Mitteilungen des Hydraulischen, Institut der Technischen Hochschule, Munich, English translation, Cornell Aeronautical Laboratory, 1949.
- TRIANTAFYLLOU, G. S. 1983 An evaluation of the hydroelastic behaviour of membranes in parallel-flow mineral-collecting systems. Ph.D. Thesis, Department of Ocean Engineering, MIT, Cambridge, MA, U.S.A.
- VENTRES, C. S. & DOWELL, E. H. 1970 Comparison of theory and experiment for nonlinear flutter of loaded plates. *AIAA Journal* **8**, 2022–2030.
- WHITE, F. M. 1991 *Viscous Fluid Flow*. New York: McGraw-Hill.

## APPENDIX: NOMENCLATURE

$A$	$H/l$ , aspect ratio
$a$	strip thickness
$B_n$	generalized damping
$C_D$	drag coefficient per unit area of the wetted surface
$C_c$	$\frac{1}{2}\pi A$ , lift coefficient due to the circulation
$C_n$	lift coefficient due to the lateral-edge vortex flow
$C_0$	drag coefficient of the straight strip in normal flow
$C_\tau$	drag coefficient due to the skin friction

$D$	$Ea^3/[12(1 - \mu^2)]$ , flexural rigidity
$E$	modulus of elasticity
$F_n$	normal aerodynamic force per unit area
$F_\tau$	tangential aerodynamic force per unit area
$f$	frequency
$g$	acceleration due to gravity
$H$	strip width
$K_n$	generalized stiffness
$k$	curvature
$l$	strip length
$M$	$\frac{1}{4}\rho\pi H$ , "added mass" of a cross-section strip
$M_n$	generalized mass
$m$	$\rho_0 a$ , strip mass in vacuum per unit area
$m^*$	$(\rho_0 - \rho)a$ , strip mass in flow per unit area
$N$	dimension of modal basis
$Q_j$	generalized coordinates
$q$	$\frac{1}{2}\rho U^2$ , dynamic pressure
$Re_s$	$Us/\nu$ , Reynolds number based on $s$
$Re$	$Ul/\nu$ , Reynolds number based on $l$
$s$	curvilinear coordinate along the strip
$T(s, t)$	dimensional tension force
$t$	time
$U$	freestream air velocity
$V$	$U(ml^2/D)^{1/2}$ , nondimensional air velocity
$v, h, w$	deflection of strip in $x, y, z$ directions
$X_1, X_2, X_3$	Cartesian coordinates in the original state of strip
$x, y, z$	Cartesian coordinates in the deformed state of strip
$n, \tau$	orthogonal system coordinates
$\gamma$	$m^*gl^3/D$ , nondimensional parameter of gravity
$\delta$	$M/m$ , spanwise mass ratio
$\varepsilon$	accuracy
$\eta$	$h/l$ , nondimensional deflection of the strip
$\lambda$	eigenvalue
$\mu$	Poisson's ratio
$\nu$	kinematic viscosity of the fluid
$\xi$	$s/l$ , nondimensional coordinate along the strip
$\rho_0, \rho$	densities of the strip and fluid, respectively
$\sigma$	$\rho l/2m$ , streamwise mass ratio
$\tilde{\tau}$	$t(D/ml^4)^{1/2}$ , nondimensional time
$\Phi_j(\xi)$	beam eigenfunctions